











# Effects of Spacing-to-Burden Ratio and Joint Angle on Rock Fragmentation: An Unmanned Aerial Vehicle and AI Approach in Overburden Benches

Dasyapu Ramesh<sup>1</sup>, Nidumukkala Sri Chandrahas<sup>1\*</sup>, Musunuri Sesa Venkatramayya<sup>2</sup>, Malothu Naresh<sup>1</sup>, Pradeep Talari<sup>1</sup>, Dhangeti Uma Venkata Durga Prasad<sup>1</sup>, Kannavena Sravan Kumar<sup>1</sup>, Vasala Vinod Kumar<sup>1</sup>

<sup>1</sup> Mining Engineering Department, Malla Reddy Engineering College, 500014 Hyderabad, India

<sup>2</sup> Mining Engineering Department, University College of Engineering, 500007 Osmania, Hyderabad, India

\* Correspondence: Nidumukkala Sri Chandrahas ([srichandrahas@mrec.ac.in](mailto:srichandrahas@mrec.ac.in))

**Received:** 08-10-2023

**Revised:** 09-01-2023

**Accepted:** 09-07-2023

**Citation:** D. Ramesh, N. S. Chandrahas, M. S. Venkatramayya, M. Naresh, P. Talari, D. U. V. D. Prasad<sup>1</sup>, K. S. Kumar, and V. V. Kumar, "Effects of spacing-to-burden ratio and joint angle on rock fragmentation: An unmanned aerial vehicle and AI approach in overburden benches," *Acadlore Trans. Geosci.*, vol. 2, no. 3, pp. 155–166, 2023. <https://doi.org/10.56578/atg020303>.



© 2023 by the authors. Licensee Acadlore Publishing Services Limited, Hong Kong. This article can be downloaded for free, and reused and quoted with a citation of the original published version, under the CC BY 4.0 license.

**Abstract:** In quarrying and mining operations, the results of the blasting process profoundly influence subsequent processes. Two primary categories dictate blast outcomes: controllable and non-controllable factors. For optimal fragmentation, it's pivotal that controllable variables, notably blast geometry and explosive attributes, are meticulously planned in correlation with non-controllable ones, such as geological aspects. In this study, the influence of blast design parameters on rock mass was investigated by examining the observable characteristics of joints and bedding planes on rock surfaces. Information extraction from these discontinuities was facilitated through cloud data processing. Within the scope of the research, 12 synchronized blasts were executed in the Basanth Nagar Limestone Mine (BNLM), tailored to its inherent joints. Results indicated that the spacing-to-burden ratio, powder factor, and joint angle significantly influenced the mean fragment size. An inverse relationship was observed between the spacing-to-burden ratio and the mean fragment size; optimal ratios for superior fragmentation were found between 1.25 and 1.3. Joint angles ranging between 75° and 80° were associated with optimal fragmentation, whereas angles exceeding 80° yielded larger rock boulders. Effective powder factors ranged from 0.36 to 0.47, with the necessity of the powder factor for rock fracturing being heavily dependent on the joint angle of the rock.

**Keywords:** Blast design parameters; Unmanned Aerial Vehicle (UAV); AI; Joints; Rock fragmentation

## 1 Introduction

The degree of rock fragmentation in blasting is of paramount concern due to its significant impact on the efficiency and cost implications of mining operations. Influenced by a myriad of factors such as the intrinsic nature of the rock, explosive properties, blast geometry, and initiation sequence, fragmentation remains a complex outcome to control. Paramount to achieving optimal fragmentation is an understanding of the rock mass, particularly given its inherent variability [1]. It has been suggested that for fragmentation control, the right amount of energy must be judiciously deployed, with rock mass characteristics considered [1].

The correlation between various determinants and the ultimate fragmentation quality holds profound importance for the progression of blasting techniques. It was posited that the efficacy and productivity of blasting are primarily gauged by fragment size [2]. The potential to elevate the productivity of mining equipment such as loaders and excavators rests on optimal blasting outcomes [3, 4]. Absence of consistent evaluation of rock fragmentation might culminate in unforeseen surges in production costs and ensuing delays [3]. With drilling and blasting accounting for a substantial 15 to 20% of total mining expenditures [5, 6], tailoring blast designs to maximize outcomes is essential [7].

A crucial parameter in this process is the spacing burden ratio, particularly in situations characterized by discontinuities [8]. The spacing, denoted by S, and described as the distance between successive holes, is affected by variables like burden (B), timing intervals between blast holes, and initiation sequence. Bench rock characteristics have been observed to influence the burden length, which can fluctuate between 20 and 40 times the diameter of the

drill hole [9]. Overly expansive spacing was found to be linked with subpar fracturing, resulting in irregular rock faces and challenges associated with the toe. On the other hand, minimized spacing was associated with excessive breakage and crater formations [10]. Fragment size has been reported to surge with increases in both spacing and burden [11]. Previous studies have highlighted that a reduced spacing-to-burden ratio, especially between 1.1 and 1.25, is correlated with a decrease in the mean fragmentation size [11]. The efficacy of subsequent processes has been noted to be directly affected by rock fragment sizes [12]. The intricate interplay between burden and spacing in the context of blast design parameters and fragmentation has been emphasized in the literature [13].

Geotechnically, rock joints stand out as vital discontinuities [14, 15]. Defined as fractures with negligible relative displacement in natural formations, the presence of these joints in rock masses introduces dynamic flexibility, altering their mechanical composition [16]. Upon encountering any form of discontinuity, stress waves were found to attenuate rapidly, experiencing a swift energy drop [16]. Investigations into the relationship between the abundance and quality of rock joints remain crucial [17]. Fragmentation was observed to be influenced significantly by the presence of joints within rock formations [18, 19]. Utilizing natural fracture lines, including joint and bedding planes, has been identified as a strategy to enhance blasting outcomes [20]. Joint spacing was reported to play a central role in determining the fragmentation pattern post-blasting. Rocks with narrower joint spacings have been recommended to be blasted using explosives possessing lower shock and higher gas energy, whereas the inverse is true for rock masses with broader joint spacings [21].

Furthermore, to joint spacing, other significant variables that affect the mean fragmentation size include joint angle [22]. When the wave front route was at an angle to the joint plane, poor rock fragmentation happened. On the other hand, excellent rock fragmentation was produced when the blast was directed in a line that was parallel to the plane of weakness. In many cases, it was discovered that better fragmentation took place when the free face was oriented parallel to the joint planes [23].

In several scientific fields, data collection employing UAV technologies has led to more accurate results [24]. The mining sector has lately utilized UAV technology to conduct volume estimates, terrain monitoring, and surveying. Using photogrammetric data, geological formations were measured and characterized [25]. A study showed how to map the locations of geological joints using photogrammetric techniques. It is feasible to collect topographic data with millimeter- to centimeter-level resolution using UAV technology over areas covering many square kilometers [26]. UAV technology is affordable and simple to operate. To analyze the strike and dip of fractures, 3D structural data are extracted from a 3D point cloud in structural analysis [27]. Yang [28] used cutting edge software and UAV datasets to find joints, faults, and fractures in dip and strike orientations. Using data from UAVs, a novel least-cost path method was also created by Hajihassani et al. [29] to map geological structures like joints. Additionally, fragmentation can be mapped with greater accuracy than with traditional methods [30]. Similar to this, computational methods nowadays also contribute significantly to the measurement and prediction of joints [31]. Combining face mapping technology with drone photos and AI software evaluation can produce the best possible fragmentation with allowed PPV [32]. Drones or unmanned aerial vehicles are excellent for finding joint planes and other geological discontinuities that could help with blast design [1].

## **2 Materials and Methods**

### **2.1 Field Data Collection**

The prospective study was conducted at the BNLM, situated in the Peddapalli District, specifically in Palakurthi Mandal, Telangana, to collect information pertaining to geo-blast design parameters. The geographic coordinates of the area are demarcated by latitudes 18°42'00" and 18°47'00", and a longitude of 79°25'00". These coordinates are visually represented in Figure 1. Convenience sampling was chosen to obtain data related to rock joints as well blast design parameters, which play a crucial role in blast designs and implementation.

The DJI MAVIC Unmanned Aerial Vehicle (UAV) was used in this investigation to capture pertinent photos of joint planes across the bench. This particular UAV had the capability to record both photos and videos at a 4K resolution and had a weight of 258 grams. It could remain airborne for up to 25 minutes on a single battery charge. Calibration procedures were carried out to address signal issues, thereby ensuring a smoother and more efficient launch of the drone. The drone was utilized to take a specific aerial shot, showcasing the blast site on the limestone, as depicted in subgraphs (a) and (b) and (c) of Figure 2. The primary purpose of deploying the UAV was to photograph the benches in an orthogonal (perpendicular) orientation both before and after the blast, facilitating subsequent fragmentation analysis.

The core objective of this drone survey was to capture high-resolution images of the joint planes, joint spacing, and the length of these joints in the vertical section of the bench. Throughout the flight, the UAV maintained an altitude of one hundred feet above the shooting bench range, with a seventy-five percent overlap to ensure comprehensive coverage. The camera angle remained fixed at 45 degrees, aimed at capturing the edge of the benchtop and the beginning of the bench floor to minimize potential errors in the images. The direction in which the photos were captured played a pivotal role in creating an accurate 3D model, which is vital for designing realistic blasts tailored to

the geological and rock conditions of the site. To facilitate efficient data collection, the intended bench was divided into three sections: the top, the bottom, and a combination of the crest and toe, as indicated in the images. This setup enabled capturing between 70 and 80 percent overlap while ensuring the highest level of precision and care in data acquisition. The UAV-captured photographs were put to use in STRAYOS SOFTWARE to generate 3D model to determine the rock joint planes which was presented in section 3 below.

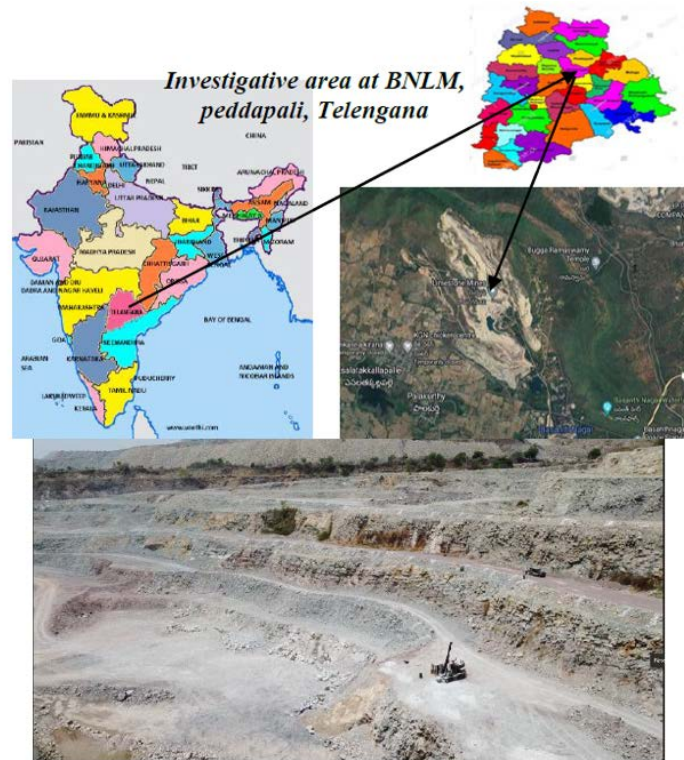


**Figure 1.** A composite of the Indian map and a Google Earth image pinpointing the location of BNLM

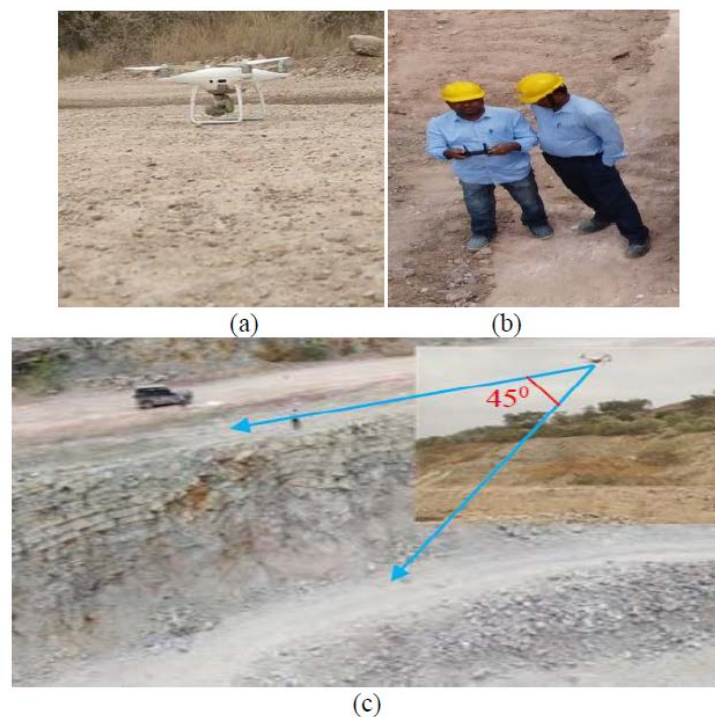


**Figure 2.** (a) Drone calibration process; (b) Drone take-off sequence; (c) Scanning of the bench area



### 3 AI Tools for Rock Characterization

AI tools have been utilized to assess the intensity and patterns of rock joints at the designated workbench, as depicted in Figure 3. The iterative examination of rock joint images was performed, seeking underlying patterns within the visual data. When joints are present within a rock mass, the transmission of blast waves can be obstructed, thereby influencing fragmentation. In specific circumstances, either the absence of back-break or over-break was noted. Such instances can foster enhanced fragmentation owing to the presence of joints, optimizing overall performance. Furthermore, it was observed that in rock masses showing signs of weakness, where explosive gases exert propulsive forces; numerous young trees might flourish proximate to these joints without inducing fractures.

The imperative to accurately characterize bench cracks is underscored by its substantial impact on the design considerations concerning blast hole spatial configurations and deck placements. For the generation of a three-dimensional model, the STRAYOS software necessitates more than ten aerial images, captured via drones. Upon data input, a three-dimensional representation of the bench is displayed, with bench photography processes illustrated in Figure 3. Utilizing AI recommendations, the activation of various clusters reveals three-dimensional planes and lines on the graphical output. The software offers dual modalities—lines and planes—for user-facilitated discontinuity analysis. When the feature visualizing cluster planes and lines is engaged, the orientation of the dip and strike, along with the dip angle of bench joints, becomes discernible, as showcased in Figure 4.

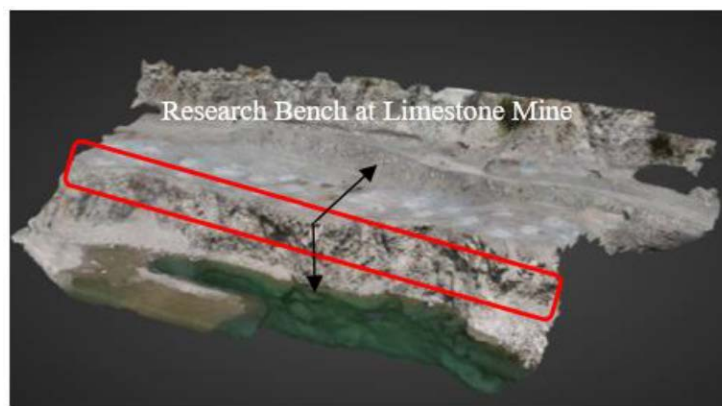


**Figure 3.** AI-generated 3D model of the workbench

Incorporating the U-Net convolution neural network model, the AI software creates a flattened three-dimensional bench model, distinctly outlining bedding planes and joints. The convolution layer, fundamental to convolution neural networks, employs filters or neurons which act on specific pixel subsets of the input data, contingent on the filter's (or kernel's) dimensions. This kernel finds utility in diverse image processing operations, such as image segmentation, adjustment, and edge detection. As the kernel traverses the image, pixel values undergo multiplication by corresponding filter values. These products are then aggregated to yield a singular value, subsequently contributing to the ensuing convolution layer. Thereafter, a maximum pooling strategy is employed within the network, serving to decrease the spatial dimension of the representation, the parameter count, and the computational overhead [1].

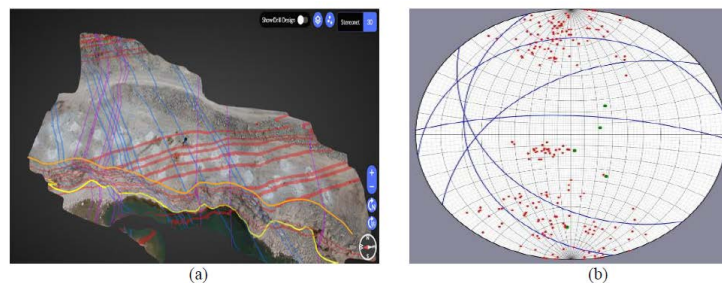


**Figure 4.** (a) AI-facilitated rock mass analysis; (b) Stereonet representations, complete with polar and coordinate data

#### 3.1 Identification of Joint Planes via UAV Imaging

To refine the newly devised blast design, a thorough assessment of rock formations and joint intensities was undertaken. The DJI Phantom UAV was selected for joint plane identification. This UAV, equipped with 4K-

resolution photographic capabilities, boasted an aerial duration of 25 minutes on a single battery charge, and had a weight of 1388 grams. Prior to deployment, a calibration process was executed to rectify potential signal discrepancies, enhancing the UAV's take-off efficacy from the runway.

Control over the drone was facilitated via a mobile application mode, leveraging 18 GPS poles. Flight trajectories were strategically planned, allowing the UAV to soar both above the bench's apex and its floor. Emphasis was placed on capturing images along paths with a minimum of 70-80% overlap, while also ensuring an overshoot of approximately 20 feet surrounding the target zone. To eliminate photographic errors, the camera was oriented at a 45° angle, prioritizing the top edge of the bench and an initial segment of the bench floor. For augmented accuracy, between four and five images were captured concurrently, facilitating the provision of multi-point cloud data. This accumulated data was subsequently processed through the STRAYOS software to construct a 3-D model.

### 3.2 AI-Guided Blast Design and Prediction

To fulfill the primary objective of the study, blasts were executed, as demonstrated in Figures 5 and Figures 6. These simulations were performed using variations in the spacing-burden ratio, as modeled in AI-based software. To ensure a comprehensive assessment, the data regarding joints, depicted in subgraph (a) of Figure 4, were integrated. Additionally, orientation data, specifically regarding planes and lines as presented in subgraph (b) of Figure 4, were also incorporated into the blast design process.

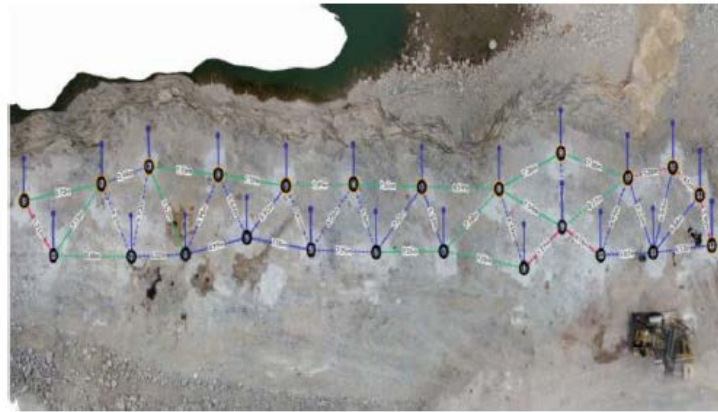


**Figure 5.** AI-simulated variations in spacing-burden ratio: Orthogonal view

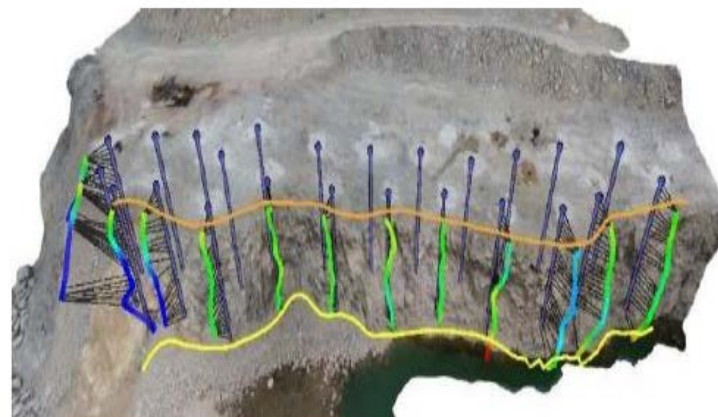


**Figure 6.** AI-simulated variations in spacing-burden ratio: Cross-sectional view relative to the bench's free face

### 3.3 Blast Design Prediction and Experimentation

To achieve the primary objective of the study, blasts were executed, designed using AI-based software. Twelve blasts were conducted on benches composed of sedimentary rocks, specifically Overburden and limestone. Various combinations of blasts were executed to examine individual trends and assess their effects on rock fragmentation. Among the blast design factors, only the Spacing Burden Ratio was adjusted in accordance with the angles of the joints.

Initially, experimental benches were cleaned to a depth of 0.3 meters to enhance joint visibility, which facilitated identification and reference marking. Such a procedure proves pivotal in mines with historical underground workings, where there is an increased propensity for fracture formation and strata disruption. An L&T 9020 Dozer was employed to clear and level the ground across all experiment benches. To maintain precision, joint markings were consistently made on every bench using appropriate scales and measurement tools. To counter potential disturbances from wind turbulence and climatic variables, markings were reinforced with white powder in a two-step process. Once joint planes were identified, careful estimations of burden and spacing were made to prevent overlapping drilling, especially where joint planes dipped.

Of the twelve standardized blasts, each was carefully documented. Post-blast, muckpiles were photographed for fragmentation analysis. Rock fragment sizes were subsequently used to plot a particle size distribution graph. Each of the twelve blasts was observed as a distinct event, and pertinent data were meticulously gathered. Drilling for blast holes followed a staggered sequence. Site Mixed Emulation (SME) explosives, such as ANFO for dry blasting, and Cartridge Emulation Explosives, were employed as blasting agents. Comprehensive measurements, including hole diameter, hole depth, burden, spacing, stem length, and charge density, were recorded. Blasts were initiated using a shock tube system at intervals of 25 ms, 42 ms, and 67 ms. In subgraph (a) of Figure 7 presents the cross-section of charged blast holes, while in subgraph (b) of Figure 7 depicts a standard firing pattern. The fragment size distribution is illustrated in Figure 8, with Figure 9 showcasing the marking strategy for drilling and subsequent explosive loading, as seen in Figure 10. A comprehensive summary of all blast experiment details can be found in Table 1.

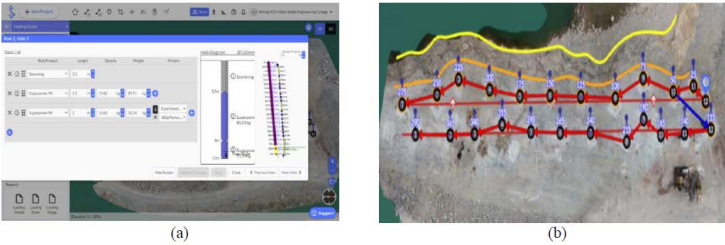


**Figure 7.** Schematic representation of hole charging and the adopted firing pattern

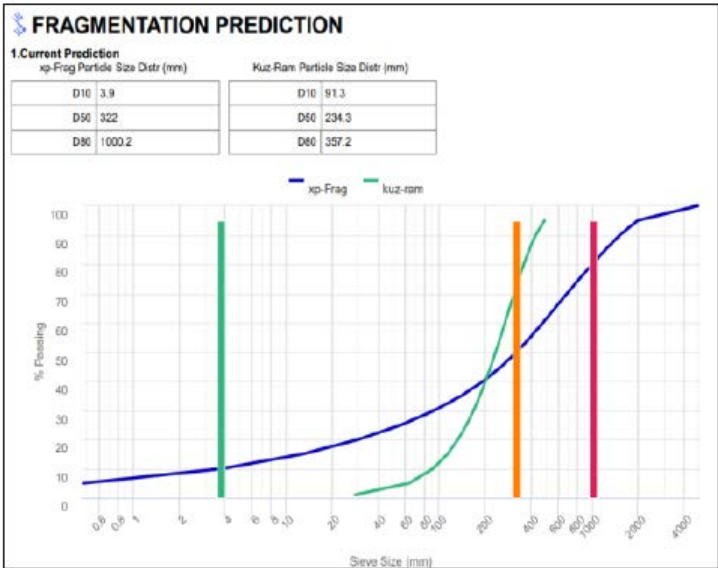


**Figure 8.** Graphical illustration of fragment size distribution following blasts

Non-electric initiation systems utilizing shock tubes have been observed to outperform the detonating fuse. This advantage primarily stems from their ability to prevent the disruption of the stemming column, thus optimizing the explosive energy within the cavity. Nonetheless, in heterogeneous strata, the use of a detonating fuse might offer better results.



**Figure 9.** Depiction of the preliminary marking strategy for bench drilling and the ensuing drilling process

**Table 1.** Compilation of blast-related data sourced from the field juxtaposed with the observed rock fragment dimensions

S.No	Blast Design Parameters	Mean	Median	Data Type
1	Bench Height (m)	10.893	10.995	Input Data
2	Hole Diameter (m)	150	150	
3	Burden (m)	4.6905	4.63	
4	Spacing (m)	6.022	6.029	
5	Hole Length (m)	11.8515	11.99	
6	Stemming Length (m)	3.805	3.9	
7	Charging Length (m)	7.7735	7.75	
8	Volume of Broken Rock (m <sup>3</sup> )	6787.65	6675	
9	Total Explosive consumed	2859.8	299.5	
10	PF Kg/m	0.4295	0.45	
11	Total charge per hole (kg)	130.85	129.5	
12	S to B ratio	1.28	1.28	Output Data
13	Joint angle	63.65	74	
14	XP-Frag Fragmentation Prediction	0.675	0.42	
15	KUZ-RAM Fragmentation Prediction	0.556	0.35	
16	AI Fragmentation analysis (m)	0.525	0.32	



**Figure 10.** Visualization of the mine's blast hole being charged using SME ANFO

### 3.4 Fragmentation Analysis via Digital Imaging

For limestone quarries, the adoption of sophisticated digital imaging technology is advocated to precisely quantify the distribution and dimensions of fragments in the resultant muck piles from blasts. It is equally paramount to underscore the vitality of on-site inspections, both antecedent to and subsequent to the blast, as these visits yield crucial insights demanding thorough analysis.

An AI-integrated software was employed, and its proficiency in meticulously discerning an exhaustive dataset representing diverse rock sizes from the ortho-photograph was verified. Subsequent to boundary demarcation, the enclosed rocks were sorted in accordance with their diameters. Values such as D10, D30, and D90 were ascertained



through the incorporation of the KUZ-RAM and SWEBREC methodologies. In a bid to diminish potential surface dust accretion on the rock, which might precipitate shadowing effects, a drone was operated at a 90-foot altitude. The camera, anchored at a direct 90-degree angle to the earth, was poised to secure images in a consistent "GRID" layout.

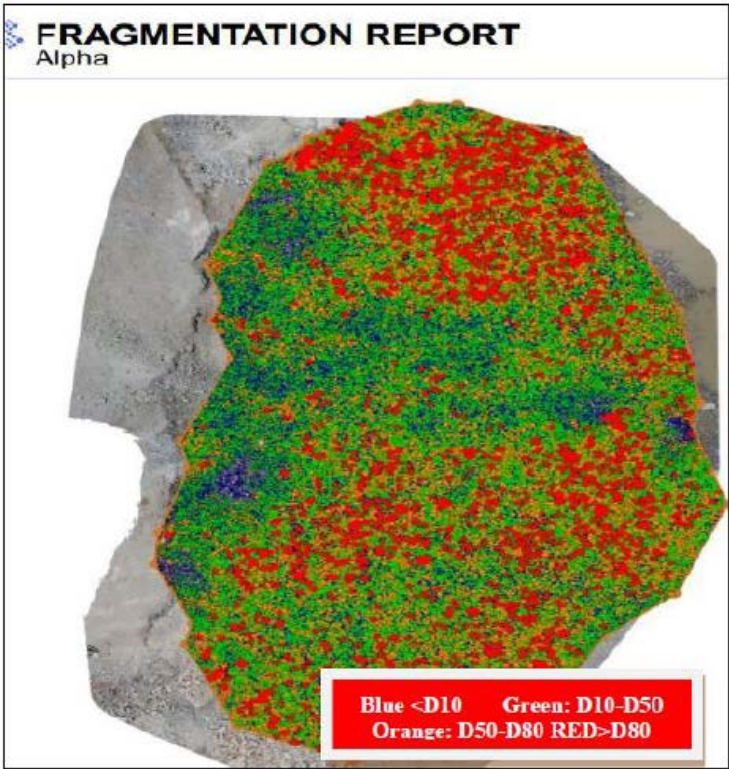


**Figure 11.** Analysis of fragmentation post-blast

This particular configuration mandated an 80% overlap among successive images. In the immediate aftermath of the detonation, during midday, the drone was dispatched to specifically canvas the expanse above the muck pile affected by the blast. The incorporated AI mechanism was adept at recognizing the debris pile’s perimeter, also conferring the flexibility to the user for any requisite boundary point adjustments. Within this demarcated domain, fragments of varying dimensions were distinguished and color-coded, as exemplified in Figure 11, with the fragment distribution subsequently illustrated in Figure 12.

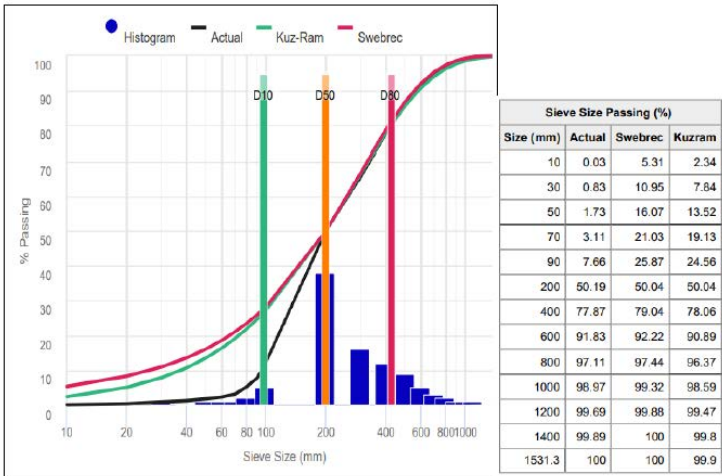


**Figure 12.** Graphical representation of fragment size distribution



## 4 Results and Discussions

### 4.1 Impact of Spacing Burden Ratio on Mean Fragmentation Size

Three distinct Spacing to Burden (S/B) ratios were employed, primarily to facilitate a more expansive spacing burden ratio when joints were observed to be parallel to the free face, as depicted in the subgraph (a) of Figure 13. Conversely, a reduced spacing burden ratio was applied where joints were perpendicular to the free face, illustrated in the subgraph (b) of Figure 13. Ratios of 1.2, 1.25, and 1.3 were scrutinized to elucidate the influence of the S/B ratio on the mean fragmentation size.

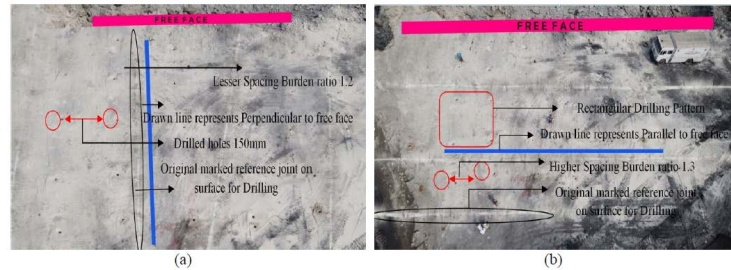


**Figure 13.** (a) Reduced spacing burden ratio in presence of joints parallel to the free face; (b) Elevated spacing burden ratio when joints are perpendicular to the free face

From the data extracted from in subgraph (a) of Figure 13, dominant joints were discerned to be parallel to the face. An increased spacing burden ratio of 1.3 was found to engender optimal fragmentation of approximately 0.4m, as shown in subgraph (b) of Figure 13. This fragmentation was attributed to the deterrence of premature joint integration and superficial crater fracturing. The peak Mean Fragmentation Size (MFS) recorded was 400mm, visualized in subgraph (a) of Figure 14.

Conversely, for vertical joints perpendicular to the excavation face, a diminished spacing burden ratio of 1.2 was associated with commendable mean fragmentation sizes, ranging between 0.4m to 0.6m. Exceptions were noted in two instances, potentially due to the interference of seismic wave reflection and refraction, which might be the result of intersections with an array of inclined joints. In these instances, the maximum MFS documented was 600mm, as highlighted in Figure 14.

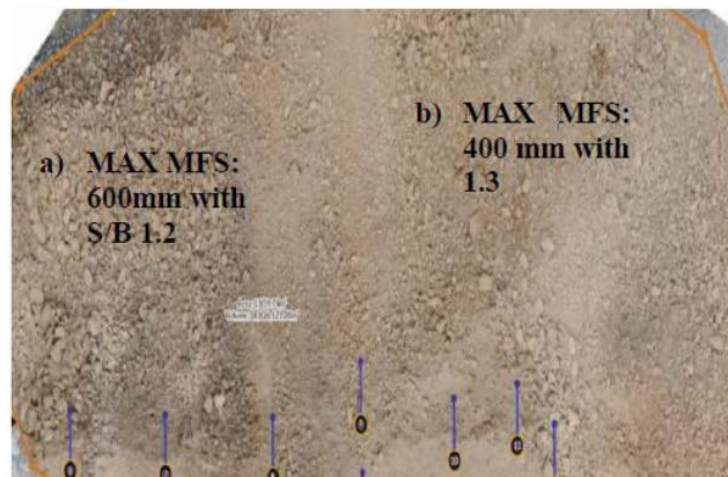


**Figure 14.** Peak MFS of 600mm observed with an S/B ratio of 1.2 contrasted against a maximum MFS of 400mm with a ratio of 1.3

Upon further analysis, particularly focusing on vertical joints perpendicular to the excavation face and with a spacing burden ratio of 1.2, fragmentation sizes predominantly fluctuated between 0.4 to 0.6. However, aberrations in two instances, potentially attributed to seismic activities influenced by multiple inclined joint intersections, recorded an elevated MFS of 800mm, as depicted in Figure 15.

### 4.2 Influence of Joint Orientation on Mean Fragmentation Size

In the observed datasets, the predominant joint patterns were identified to exhibit angles that varied from 0 degrees (aligned with the blast face) to 90 degrees (perpendicular to the bench face). Through examination of the

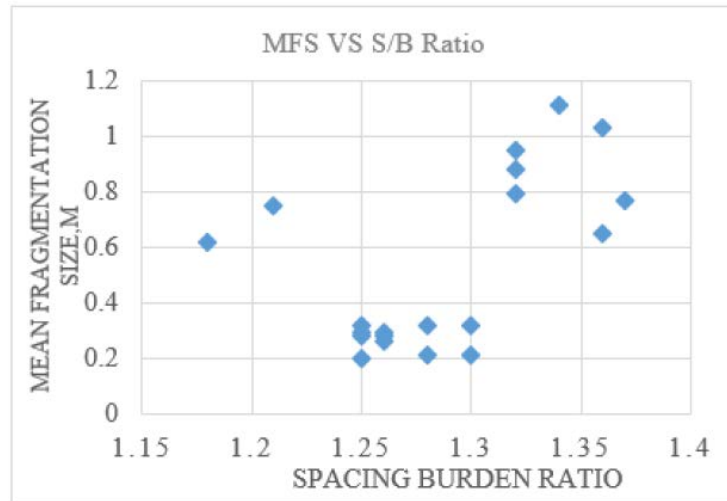


**Figure 15.** Correlation between MFS and the spacing to burden ratio

blast trials, it was determined that reduced MFS values were consistently associated with joints oriented between 70 and 90 degrees, as illustrated in Figure 16. This phenomenon can be attributed to the optimal utilization of blast energy during the complete collision of both propagating and reflecting shock waves, thereby leading to enhanced blasting outcomes and diminished MFS.

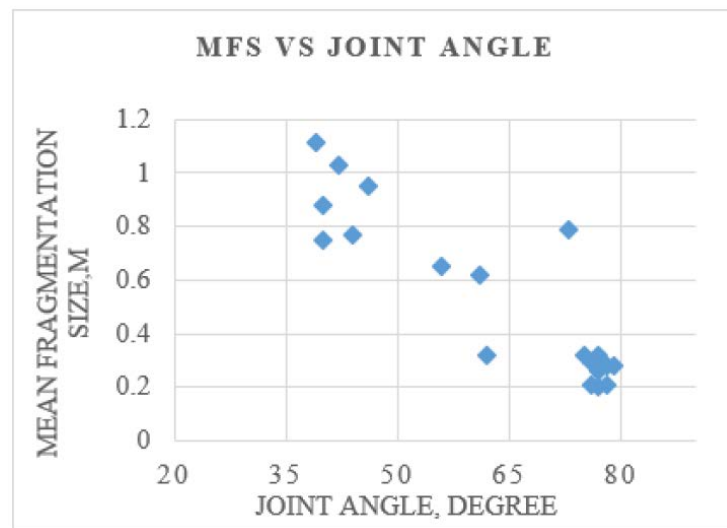


**Figure 16.** Correlation between MFS and the orientation angle of joints

## 5 Conclusions

In alignment with the research objectives, blast designs incorporating scientifically validated spacing-burden ratios were meticulously tailored to accommodate the unique presence of joints at the bench. At the limestone mine, a total of 12 impeccable blast designs were executed to elucidate the influence and trend of geological discontinuities, notably joints, on mean fragmentation size. The findings of this investigation can be summarized as follows:

- The utility of the DJI Phantom PRO was underscored by its pivotal role in capturing images in challenging terrains.
- The application of AI-driven tools proved instrumental in the delineation of joints, optimization of blast design, and the prediction and assessment of fragmentation.
- A discernible trend was identified wherein rock fragmentation size diminished as the S/B ratio (spacing-to-burden) escalated. In a majority of the cases, a spacing-to-burden ratio fluctuating between 1.25 and 1.3 was found optimal, yielding superior fragmentation outcomes within the range of 0.15 to 0.3m.
- Joint orientations, particularly angles between 75 and 80 degrees, were associated with favorable fragmentation

outcomes spanning 0.15 to 0.3m. Joint angles exceeding 70 degrees, however, were observed to result in the formation of rock boulders.

•An optimal powder factor ranged between 0.36 and 0.47 was achieved when the joint angle varied from 75 to 79 degrees, accompanied by a spacing-burden ratio oscillating between 1.25 and 1.3.

#### Data Availability

The data used to support the findings of this study are available from the corresponding author upon request.

#### Conflicts of Interest

The authors declare that they have no conflicts of interest.

#### References

- [1] N. S. Chandrabhas, B. S. Choudhary, M. V. Teja, M. S. Venkataramayya, and N. S. R. K. Prasad, "XG boost algorithm to simultaneous prediction of rock fragmentation and induced ground vibration using unique blast data," *Appl. Sci.*, vol. 12, no. 10, p. 5269, 2022. <https://doi.org/10.3390/app12105269>
- [2] B. S. Choudhary, "Firing patterns and its effect on muckpile shape parameters and fragmentation in quarry blasts," *Int. J. Res. Eng. Technol.*, vol. 2, no. 9, pp. 32–45, 2013. <https://doi.org/10.15623/ijret.2013.0209005>
- [3] B. Elevli, I. Topal, and S. Elevli, "Multivariate statistics application in development of blast fragmentation charts for different rock formations in quarries," *Acta MontanisticaSlovaca*, vol. 17, no. 4, pp. 300–309, 2012.
- [4] S. Prasad, B. Choudhary, and A. Mishra, "Effect of stemming to burden ratio and powder factor on blast induced rock fragmentation–A case study," *IOP Conf. Ser.: Mater. Sci. Eng.*, vol. 225, pp. 298–311, 2017. <https://doi.org/10.1088/1757-899x/225/1/012191>
- [5] P. Kulatilake, W. Qiong, T. Hudaverdi, and C. Kuzu, "Mean particle size prediction in rock blast fragmentation using neural networks," *Eng. Geol.*, vol. 114, no. 3-4, pp. 298–311, 2010. <https://doi.org/10.1016/j.enggeo.2010.05.008>
- [6] B. Bozic, "Control of fragmentation by blasting," *Rudarsko – Geolosko - NaftniZbornik*, vol. 10, no. 1, pp. 49–57, 1998.
- [7] S. S. Kanchibotla, S. Morrell, W. Valery, and P. Loughlin, "Exploring the effect of blast design on SAG mill throughput at KCGM," in *Proceedings of Mine to Mill Conference, Australasian Institute of Mining and Metallurgy*, 1998, pp. 153–158.
- [8] E. F. Salmi and E. J. Sellers, "A review of the methods to incorporate the geological and geotechnical characteristics of rock masses in blastability assessments for selective blast design," *Eng. Geo.*, vol. 281, p. 105970, 2021. <https://doi.org/10.1016/j.enggeo.2020.105970>
- [9] A. Chakraborty, J. Jethwa, and A. Paithankar, "Assessing the effects of joint orientation and rock mass quality on fragmentation and overbreak in tunnel blasting," *Tunn. Undergr. Sp. Tech.*, vol. 9, no. 4, pp. 471–482, 1994. [https://doi.org/10.1016/0886-7798\(94\)90106-6](https://doi.org/10.1016/0886-7798(94)90106-6)
- [10] P. K. Singh, M. P. Roy, R. K. Paswan, M. Sarim, S. Kumar, and R. Ranjan Jha, "Rock fragmentation control in opencast blasting," *J. Rock Mech. Geotech.*, vol. 8, no. 2, pp. 225–237, 2016. <https://doi.org/10.1016/j.jrmge.2015.10.005>
- [11] L. Frankel, "Relative rates of loess deposition in Nebraska," *J. Geol.*, vol. 65, no. 6, pp. 649–652, 1957.
- [12] S. Reddy, A. K. Tripathi, and S. Parida, "Influence of stemming material on performance of blasting," *PalArch's J. Archaeol. Egypt/Egyptology*, vol. 17, no. 7, pp. 9797–9809, 2020.
- [13] G. H. Davis, S. J. Reynolds, and C. F. Kluth, *Structural Geology of Rocks and Regions (3rd ed.)*. John Wiley and Sons, Inc., 2012.
- [14] A. S. Goudie, *Encyclopedia of Geomorphology volume 2 J–Z*. Routledge New York, 2004.
- [15] R. E. Goodman, L. Taylor, and T. L. Brekke, "A model for the mechanics of jointed rock," *J. Soil Mech. Found Div.*, vol. 1968, pp. 637–659, 1968.
- [16] W. C. Burkle, "Geology and its effect on blasting," in *Proceedings of the 5th Conference on Explosives and Blasting Techniques*, 1979, pp. 105–120.
- [17] P. Cundall, "Numerical modelling of jointed and faulted rock," *Mechanics of Jointed and Faulted Rock*, pp. 11–18, 2020.
- [18] P. Rai and H. S. Yang, "Investigation of some blast design and evaluation parameters for fragmentation in limestone quarries," *Tunnel Undergr. Sp.*, vol. 20, no. 3, pp. 183–193, 2010.
- [19] S. Chandrabhas, B. S. Choudhary, N. S. R. K. Prasad, V. Musunuri, and K. K. Rao, "An investigation into the effect of rockmass properties on mean fragmentation," *Arch. Min. Sci.*, vol. 66, no. 4, 2021.



- [20] S. Xu, Y. Li, J. Liu, and F. Zhang, "Optimization of blasting parameters for an underground mine through prediction of blasting vibration," *J. Vib. Control*, vol. 25, no. 9, pp. 1585–1595, 2019. <https://doi.org/10.1177/1077546319829938>
- [21] J. M. Belland, "Structure as a control in rock fragmentation coal lake iron ore deposited," *The Canadian Min. Metall. Bull.*, vol. 59, no. 647, pp. 323–328, 1968.
- [22] K. Talhi and B. Bensaker, "Design of a model blasting system to measure peak p-wave stress," *Soil Dyn. Earthq. Eng.*, vol. 23, no. 6, pp. 513–519, 2003. [https://doi.org/10.1016/s0267-7261\(03\)00018-6](https://doi.org/10.1016/s0267-7261(03)00018-6)
- [23] D. Turner, A. Lucieer, and C. Watson, "An automated technique for generating georectified mosaics from ultra-high resolution Unmanned Aerial Vehicle (UAV) imagery, based on Structure from Motion (SfM) point clouds," *Remote Sens.*, vol. 4, no. 5, pp. 1392–1410, 2012. <https://doi.org/10.3390/rs4051392>
- [24] T. Bamford, K. Esmaeili, and A. P. Schoellig, "A real-time analysis of post-blast rock fragmentation using UAV technology," *Int. J. Min., Reclam. Env.*, vol. 31, no. 6, pp. 439–456, 2017. <https://doi.org/10.1080/17480930.2017.1339170>
- [25] J. Kottenstette, "Measurement of geologic features using close range terrestrial photogrammetry," in *Proceedings of the 40th US Symposium on Rock Mechanics (USRMS) Alaska Rocks*, vol. 2005, 2005. <https://search.spe.org/i2kweb/SPE/doc/onepetro:C7153EC8>
- [26] Y. Vasuki, E. J. Holden, P. Kovesi, and S. Micklethwaite, "Semi-automatic mapping of geological Structures using UAV-based photogrammetric data: An image analysis approach," *Comput. Geosci.*, vol. 69, pp. 22–32, 2014. <https://doi.org/10.1016/j.cageo.2014.04.012>
- [27] S. Thiele, L. Grose, A. Samsu, S. Micklethwaite, S. A. Vollgger, and A. R. Cruden, "Rapid, semi-automatic fracture and contact mapping for point clouds, images and geophysical data," *Solid Earth*, vol. 8, no. 6, pp. 1241–1253, 2017. <https://doi.org/10.5194/se-8-1241-2017>
- [28] X. S. Yang, "Firefly algorithms for multimodal optimization," in *International Symposium on Stochastic Algorithms*, 2009, pp. 169–178.
- [29] M. Hajihassani, D. J. Armaghani, M. Monjezi, M. E. Tonnizam, and A. Marto, "Blast-induced air and ground-vibration prediction: A particle swarm optimization-based artificial neural network approach," *Environ. Earth Sci.*, vol. 74, no. 4, pp. 2799–2817, 2015.
- [30] W. K. Chen, *Linear Networks and Systems*. Wadsworth, Belmont, 1993, pp. 123–135.
- [31] T. Costa, P. Zarante, and J. Sodre, "Simulation of aldehyde formation in ethanol fuelled spark ignition engines," in *International Engine Process Conference*, 2013, pp. 112–122.
- [32] R. E. Bentley, *Handbook of Temperature Measurement Vol. 3: The Theory and Practice of Thermoelectric Thermometry*. Springer Science & Business Media, 1998.